doi:10.1038/nature06717

LETTERS

X-ray structure of a prokaryotic pentameric ligand-gated ion channel

Ricarda J. C. Hilf[1] & Raimund Dutzler[1]

Pentameric ligand-gated ion channels (pLGICs) are key players in the early events of electrical signal transduction at chemical synapses. The family codes for a structurally conserved scaffold of channel proteins that open in response to the binding of neurotransmitter molecules. All proteins share a pentameric organization of identical or related subunits that consist of an extracellular ligand-binding domain followed by a transmembrane channel domain. The nicotinic acetylcholine receptor (nAChR) is the most thoroughly studied member of the pLGIC family (for recent reviews see refs 1–3). Two sources of structural information provided an architectural framework for the family. The structure of the soluble acetylcholine-binding protein (AChBP) defined the organization of the extracellular domain and revealed the chemical basis of ligand interaction[4–6]. Electron microscopy studies of the nAChR from *Torpedo* electric ray have yielded a picture of the full-length protein and have recently led to the interpretation of an electron density map at 4.0 Å resolution[7–9]. Despite the wealth of experimental information, high-resolution structures of any family member have so far not been available. Until recently, the pLGICs were believed to be only expressed in multicellular eukaryotic organisms. The abundance of prokaryotic genome sequences, however, allowed the identification of several homologous proteins in bacterial sources[10,11]. Here we present the X-ray structure of a prokaryotic pLGIC from the bacterium *Erwinia chrysanthemi* (ELIC) at 3.3 Å resolution. Our study reveals the first structure of a pLGIC at high resolution and provides an important model system for the investigation of the general mechanisms of ion permeation and gating within the family.

ELIC is similar in length and sequence to its orthologue from the cyanobacterium *Gloebacter violaceous* (sharing 18% of identical amino acids) and it shows considerable homology to eukaryotic family members (with 16% sequence identity to nAChRα, Supplementary Fig. 1). When investigated in artificial lipid bilayers, the protein mediates cation-selective currents but it does not discriminate between different monovalent cations such as Na^+, K^+ and Cs^+, a functional behaviour that closely resembles the selectivity of acetylcholine and serotonin receptors[12] (Supplementary Fig. 2). The crystal structure of ELIC has been determined at 3.3 Å resolution by the SIRAS (single isomorphous replacement anomalous scattering) method (Supplementary Table 1, and Supplementary Figs 3 and 4). The pentameric protein is shown in Fig. 1. The five subunits are arranged like the staves of a barrel around a symmetry axis that defines the ion permeation path. The overall dimensions of the protein (95 Å × 110 Å) closely resemble the acetylcholine receptor ion channel, not including the cytoplasmic region, which is absent in ELIC. The subunits are tightly interacting in both, their extracellular and their membrane embedded part with adjacent subunits burying more than 5,000 $Å^2$ of the combined molecular surface. On the extracellular side, the protein subunits enclose a wide, aqueous, cylindrical vestibule with a diameter of about 16 Å that is lined by charged and hydrophilic residues. This vestibule narrows down at the membrane interface to a discontinuous, partly hydrophobic pore with a maximum diameter of about 7 Å that probably defines a closed conformation of the channel.

Each protein subunit is organized in two halves: the amino-terminal half that constitutes the extracellular domain and a carboxy-terminal half that makes up the pore domain (Fig. 1c). Both termini of the protein chain are located on the extracellular side. The extracellular domain consists of ten β-strands that are organized in two sheets to form a β-sandwich and a short α-helix. The topological organization of the extracellular domain of ELIC is very similar to its eukaryotic counterparts and to AChBP, except for an N-terminal α-helix that is abundant in eukaryotic proteins and missing in bacterial pLGICs. The regions of conserved sequence include the central part of the 'Cys-loop' that connects β6 and β7 but does not extend to the flanking disulphide-bridged cysteinse residues that are strictly conserved among eukaryotic pLGICs (Supplementary Fig. 1a). The transmembrane region consists of four α-helices that are connected by short loops. These four helices (named α1–α4) are equivalent to the previously described transmembrane regions M1–M4 of the acetylcholine receptor[8]. Three helices (α1–α3) span the membrane with small tilts with respect to its plane and form a tightly interacting bundle. In the pentameric protein, these helices are arranged in two concentric layers around the pore axis: an inner circle that is formed by helix α2 and an outer circle defined by the helices α1 and α3. Only residues of α2 contribute to the pore lining, whereas α1 and α3 appear to shield and stabilize the pore. All three segments are involved in interactions at subunit interfaces, whereas the fourth helix, α4, is located at the periphery of this barrel-like arrangement; it only loosely interacts with α1 and α3 and is not involved in subunit–subunit interactions (Fig. 1a). In an attempt to study the interaction of monovalent cations with ELIC, we soaked our crystals in solutions that only contain the respective cation, and we identified the bound ions by anomalous and isomorphous difference Fourier techniques (Supplementary Table 2). In that way, we studied the binding of Rb^+, Cs^+ and Tl^+ ions to the protein, which have been shown to permeate through ELIC and the related nAChR channels[12] (Supplementary Fig. 2c, d). Although this approach did not allow the identification of specific binding sites in the pore region, it revealed ordered binding of ions to sites in the extracellular ligand-binding domain (Supplementary Fig. 5).

The conservation in the extracellular part of ELIC becomes evident when comparing its structure with the structure of the homopentameric AChBP, which has proved to be a valuable representative for the ligand-binding domain[4]. A superposition of the two domains is shown in Fig. 2a. Three hundred and fifty Cα positions at the N-terminal half of the ligand-binding domain of the five subunits superimpose with a root mean square deviation of less than 1.5 Å. The largest differences are found in loop regions that interact with the transmembrane channel

[1]Department of Biochemistry, University of Zürich, Winterthurer Strasse 190, CH-8057 Zürich, Switzerland.

and which are naturally absent in the soluble binding protein. The ligand-binding site of AChBP that is also conserved among acetylcholine receptors is located in a pocket of the protein at the interface between two adjacent subunits (Fig. 2a). This pocket is covered on one side by an extended loop region connecting β9 and β10. In ELIC, the tip of this loop is mobile and thus only weakly defined in its electron density, which is consistent with the increased mobility of this region that has been reported for AChBP in the absence of bound ligand[6]. Although the ligands that trigger pore opening in ELIC have not yet been identified, it is interesting to compare the structures of the equivalent regions. The acetylcholine-binding site contains conserved aromatic amino acids from dispersed regions of the protein, which contribute to an aromatic-binding pocket for quaternary ammonium compounds that are stabilized by so-called 'cation–π' interactions[5,13] (Supplementary Fig. 6a). Although the ligand-promoting channel opening in ELIC could be as small as a proton, as has been suggested for the homologous Glvi channel[11], it is remarkable to find several of these aromatic residues conserved in the ELIC structure (Fig. 2b and Supplementary Fig. 6b). Ordered binding of Cs^+ and Tl^+ ions emphasizes the electrostatic attraction for cations in this region and underscores its role as a potential ligand-binding site that could promote channel opening like in eukaryotic pLGICs.

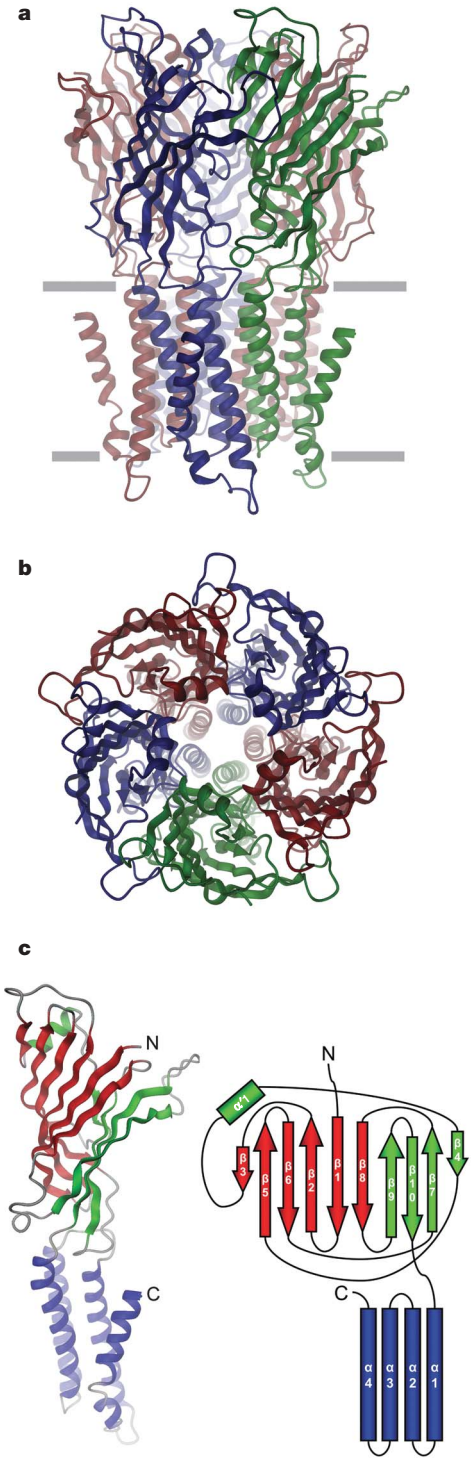

Figure 1 | ELIC structure. **a**, Ribbon representation of ELIC viewed from within the membrane with the extracellular solution above. The approximate membrane boundaries are indicated. **b**, Structure of the pentameric channel viewed from the extracellular side. **c**, Structure and topology of the ELIC subunit. The subunit is viewed from within the membrane. Secondary structure elements constituting the two sheets of the β-sandwich of the extracellular domain are coloured in red and green, respectively. The four helices of the pore region are coloured in blue. Figures 1–3 were prepared with DINO (http://www.dino3d.org).

Ligand-dependent gating involves the transduction of conformational rearrangements from the ligand-binding domain to the pore[2,14]. This process is mediated through interfacial contacts between the two domains[9]. The interface between the extracellular and pore domains is well defined in the ELIC structure and it involves, next to the covalent connection between β10 and α1, residues of three loop regions in the extracellular domain that contact the α2–α3 loop of the pore domain (Fig. 2c and Supplementary Fig. 6c). These interactions include conserved residues of the β6–β7 loop (the 'Cys' loop) and contacts to the β1–β2 turn and the β8–β9 loop of the neighbouring subunit. Several of those regions have previously been identified as influencing gating in different family members[2,15–17].

The wide and hydrophilic extracellular vestibule of ELIC leads into a narrow pore at the membrane boundary. The lumen of this pore is lined by residues of helix α2 that spans the membrane in a nearly perpendicular orientation. On its extracellular half, the pore is interrupted by bulky side chains that occlude a hydrophobic cavity that extends towards the centre of the membrane (Fig. 3a). This cavity is confined by Phe 246 on the extracellular side and by Leu 239 towards the cytoplasm. Below the constriction, a hydrophilic channel of width 6 Å leads from the membrane centre to the intracellular exit. The bulky hydrophobic side chains of Phe 246 and Leu 239 would prevent the diffusion of ions and thus probably serve as physical gates in the closed conformation of the channel. Unlike other ion-channel proteins that specifically bind the transported ions in narrow selectivity filters[18,19], we did not identify ordered binding of permeant ions in the pore of ELIC. However, we did observe binding of apolar Xe atoms in the hydrophobic cavity and at the extracellular side of Phe 246, thus underlining the hydrophobic nature of this region (Fig. 3a). When comparing the pore of ELIC with the structure of the equivalent region of nAChR, interesting differences become apparent. Unlike our structure, nAChR shows a continuous channel with a diameter of about 6 Å (ref. 9) (Fig. 3b and Supplementary Fig. 7). The difference in the pore size is most pronounced at the extracellular entry where the helices of nAChR are bent away from the channel axis, thus providing an aqueous funnel-shaped path in a region where the ELIC pore is occluded. On the intracellular side, the pore radius in both proteins is similar. This observation is in contrast to electrophysiological experiments on nAChR, which predicted a constriction towards the cytoplasm[20,21]. Apart from differences in the diameter, other features of the pore, such as the predominantly hydrophobic region at the membrane centre and the presence of acidic residues on both sides of the membrane boundary appear preserved.

An investigation of the electrostatic potential along the ion permeation path of ELIC reveals insight into the cation selectivity of the channel (Fig. 3b). The predominant negative potential throughout the channel results from the excess of acidic residues in the protein, which provide an attractive environment for cations despite the

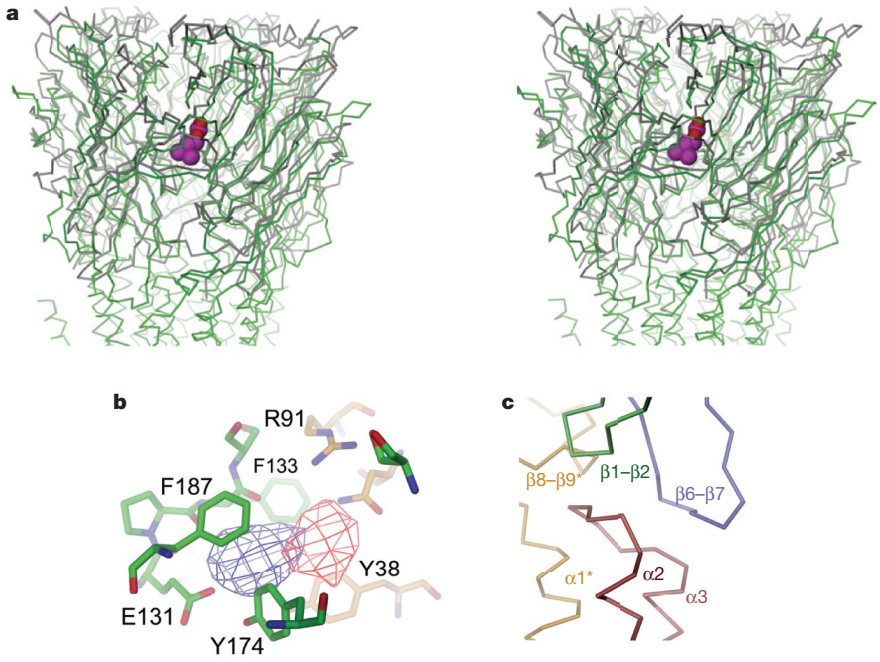

Figure 2 | Structure of the extracellular domain. **a**, Stereo view of AChBP (PDB code 1UV6) superimposed on the extracellular domain of ELIC. Proteins are shown as Cα representation and coloured in grey (AChBP) and green (ELIC). Carbamylcholine that is specifically bound to the acetylcholine-binding site of AChBP is shown as spacefilling model (carbon atoms in magenta). **b**, View of the putative ligand-binding site in ELIC. Carbon atoms of residues from the two subunits are coloured in green and orange, respectively. Selected residues are labelled. Anomalous difference electron density of bound Tl^+ and Cs^+ ions is contoured at 4σ and shown in blue and red, respectively. **c**, Cα representation of the interface region between the extracellular domain and the pore. The different elements are shown in unique colours, the 'Cys loop' (β6–β7) is coloured in blue. Residues of the neighbouring subunit are coloured in orange.

presence of positively charged residues in the extracellular vestibule, some of which are found close to the channel entrance. The electrostatic potential in the narrow pore region is dominated by acidic residues at the membrane boundary (for example, Glu 229 at the intracellular entrance). Because of the long-range nature of coulombic interactions and the low-dielectric environment of the membrane, the

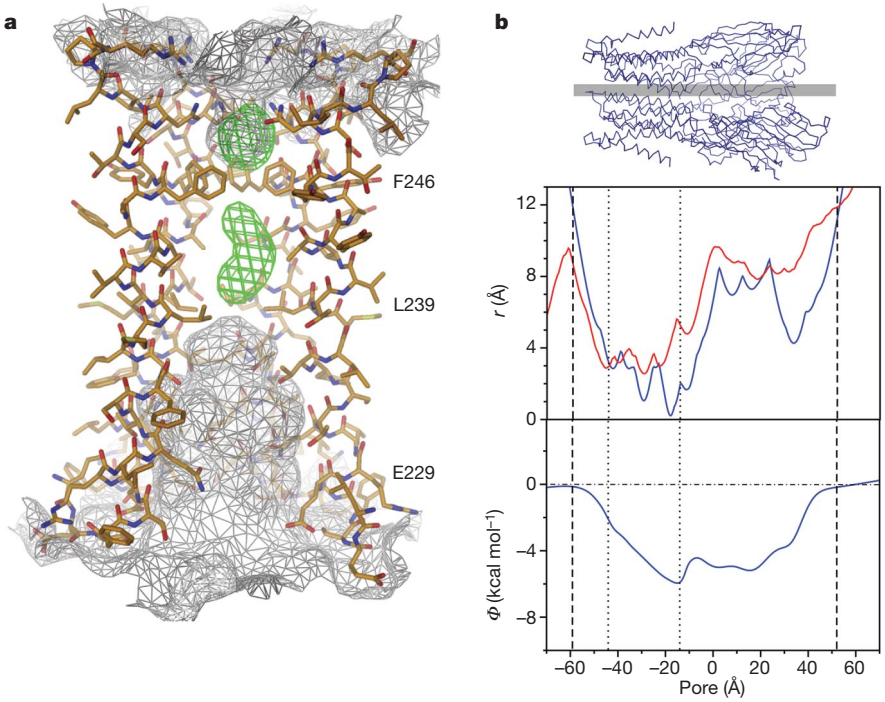

Figure 3 | ELIC pore. **a**, View of the α2 helices defining the pore region. The front subunit is removed for clarity. The molecular surface is shown as white mesh. Anomalous difference density of Xe atoms is contoured at 4σ and shown as green mesh. The positions of selected residues are indicated. **b**, Pore radius and electrostatic potential in the ELIC pore. Orientation of the ELIC channel is shown above. Molecular boundaries (dashed line) and transmembrane region (dotted line) are indicated. Top: pore radius of ELIC (blue) and nAChR (red) are shown. Bottom: electrostatic potential along the pore axis of ELIC as calculated from a numerical solution of the linearized Poisson–Boltzmann equation.

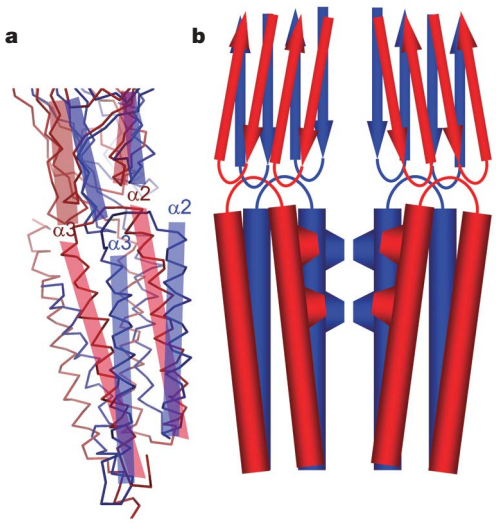

Figure 4 | Schematic model of pore opening. a, Superposition of selected regions from a single subunit of ELIC (blue) and the α-subunit of nAChR (red) close to the pore region. Differences in the helix tilt and the conformation of contacting groups from the extracellular region are highlighted. **b**, Schematic representation of two subunits, indicating a possible pore opening mechanism by a tilt of the helix at the extracellular side away from the pore axis in response to changes in the extracellular domain.

electrostatic potential in the channel is negative even though hydrophobic residues line the central pore region. This mechanism of electrostatic screening does not require the strict conservation of amino acids and may account for the fact that, although the pore regions of different family members are only weakly conserved, there is a common overall organization of hydrophobic residues in the centre and of charged residues at the periphery of the channel[22]. These charged residues have indeed been shown to confer ion selectivity to nAChR and other members of the family[23–27]. Although such a channel architecture allows for a discrimination of ions based on their charge, it does not allow for exquisite selectivity between two similar ions as found in K^+ channels[18].

Large hydrophobic residues in the centre of the pore have previously been shown to play an important role in channel closing in nAChR[8,20,28]. It has been proposed that these hydrophobic residues would impede ion permeation by a process called 'hydrophobic gating' as long as the channel does not exceed a certain size[29]. Unlike in the structure of nAChR, which shows a narrow but continuous pore, in ELIC these residues physically obstruct the channel. It will thus be interesting to see the conformational rearrangements leading to channel opening.

Different mechanisms of gating of pLGICs have been proposed in previous studies[8,21,30]. Although we do not want to engage in speculation about gating in the absence of additional data, it is interesting to compare the different conformations of the pore helices in ELIC and nAChR (Fig. 4). Both structures are believed to represent closed conformations of the respective proteins. If, however, the nAChR structure were to show a conformation that is closer to the structure of a conducting state, the difference might hint at a possible opening mechanism by an outward tilt of the pore helices on the extracellular side away from the channel axis (Fig. 4). This movement would be triggered by ligand binding to the extracellular domain and would be transmitted through the domain–domain interface.

The structure of ELIC shows the pore of a pLGIC in a non-conducting conformation. The protein shares many conserved features with its eukaryotic counterparts, which suggests that the basic mechanisms of ion permeation and gating are preserved across the prokaryotic–eukaryotic species boundary. Future studies will have to identify the ligands that promote channel opening and show the structure of a conducting conformation.

METHODS SUMMARY

ELIC was expressed in *Escherichia coli* with its N terminus fused to maltose-binding protein (MBP) preceded by a signal sequence (PelB). The protein was purified from isolated membranes in the detergent *n*-undecyl-β-D-maltoside. MBP was cleaved during purification by proteolytic digestion at a specific protease cleavage site located between MBP and the channel protein. Crystals were grown at pH 6.5 with addition of 13% PEG 4000, 200 mM ammonium sulphate and 0.5 mg ml^{-1} *E. coli* lipids. Data were collected at the X06-SA beamline at the Swiss Light Source of the Paul Scherrer Institute on a Pilatus detector (Dectris) (Supplementary Tables 1 and 2). The crystals were of space group $P2_1$ with two homo-pentameric channels in the asymmetric unit (Supplementary Fig. 4). The structure was determined by the SIRAS method, and phases were extended by cyclic tenfold non-crystallographic symmetry (NCS) averaging (Supplementary Fig. 3). All subunits were structurally very similar and were refined by maintaining strong constraints throughout (Supplementary Table 1). The final structure encompassing residues 11–316 was well refined, with good stereochemistry and no outliers in disallowed regions of the Ramachandran plot. For electrophysiological characterization in artificial lipid bilayers, the protein was reconstituted into liposomes and studied in a bilayer system.

Full Methods and any associated references are available in the online version of the paper at www.nature.com/nature.

Received 17 October 2007; accepted 15 January 2008.
Published online 5 March 2008.

1. Karlin, A. Emerging structure of the nicotinic acetylcholine receptors. *Nature Rev. Neurosci.* **3,** 102–114 (2002).
2. Lester, H. A., Dibas, M. I., Dahan, D. S., Leite, J. F. & Dougherty, D. A. Cys-loop receptors: new twists and turns. *Trends Neurosci.* **27,** 329–336 (2004).
3. Sine, S. M. & Engel, A. G. Recent advances in Cys-loop receptor structure and function. *Nature* **440,** 448–455 (2006).
4. Brejc, K. *et al.* Crystal structure of an ACh-binding protein reveals the ligand-binding domain of nicotinic receptors. *Nature* **411,** 269–276 (2001).
5. Celie, P. H. *et al.* Nicotine and carbamylcholine binding to nicotinic acetylcholine receptors as studied in AChBP crystal structures. *Neuron* **41,** 907–914 (2004).
6. Hansen, S. B. *et al.* Structures of *Aplysia* AChBP complexes with nicotinic agonists and antagonists reveal distinctive binding interfaces and conformations. *EMBO J.* **24,** 3635–3646 (2005).
7. Unwin, N. Structure and action of the nicotinic acetylcholine receptor explored by electron microscopy. *FEBS Lett.* **555,** 91–95 (2003).
8. Miyazawa, A., Fujiyoshi, Y. & Unwin, N. Structure and gating mechanism of the acetylcholine receptor pore. *Nature* **423,** 949–955 (2003).
9. Unwin, N. Refined structure of the nicotinic acetylcholine receptor at 4 Å resolution. *J. Mol. Biol.* **346,** 967–989 (2005).
10. Tasneem, A., Iyer, L. M., Jakobsson, E. & Aravind, L. Identification of the prokaryotic ligand-gated ion channels and their implications for the mechanisms and origins of animal Cys-loop ion channels. *Genome Biol.* **6,** R4 (2005).
11. Bocquet, N. *et al.* A prokaryotic proton-gated ion channel from the nicotinic acetylcholine receptor family. *Nature* **445,** 116–119 (2007).
12. Adams, D. J., Dwyer, T. M. & Hille, B. The permeability of endplate channels to monovalent and divalent metal cations. *J. Gen. Physiol.* **75,** 493–510 (1980).
13. Gallivan, J. P. & Dougherty, D. A. Cation–pi interactions in structural biology. *Proc. Natl Acad. Sci. USA* **96,** 9459–9464 (1999).
14. Purohit, P., Mitra, A. & Auerbach, A. A stepwise mechanism for acetylcholine receptor channel gating. *Nature* **446,** 930–933 (2007).
15. Campos-Caro, A. *et al.* A single residue in the M2–M3 loop is a major determinant of coupling between binding and gating in neuronal nicotinic receptors. *Proc. Natl Acad. Sci. USA* **93,** 6118–6123 (1996).
16. Grosman, C., Salamone, F. N., Sine, S. M. & Auerbach, A. The extracellular linker of muscle acetylcholine receptor channels is a gating control element. *J. Gen. Physiol.* **116,** 327–340 (2000).
17. Kash, T. L., Jenkins, A., Kelley, J. C., Trudell, J. R. & Harrison, N. L. Coupling of agonist binding to channel gating in the $GABA_A$ receptor. *Nature* **421,** 272–275 (2003).
18. Zhou, Y., Morais-Cabral, J. H., Kaufman, A. & MacKinnon, R. Chemistry of ion coordination and hydration revealed by a K^+ channel–Fab complex at 2.0 Å resolution. *Nature* **414,** 43–48 (2001).
19. Dutzler, R., Campbell, E. B. & MacKinnon, R. Gating the selectivity filter in ClC chloride channels. *Science* **300,** 108–112 (2003).
20. Wilson, G. & Karlin, A. Acetylcholine receptor channel structure in the resting, open, and desensitized states probed with the substituted-cysteine-accessibility method. *Proc. Natl Acad. Sci. USA* **98,** 1241–1248 (2001).
21. Paas, Y. *et al.* Pore conformations and gating mechanism of a Cys-loop receptor. *Proc. Natl Acad. Sci. USA* **102,** 15877–15882 (2005).
22. Le Novere, N. & Changeux, J. P. LGICdb: the ligand-gated ion channel database. *Nucleic Acids Res.* **29,** 294–295 (2001).
23. Konno, T. *et al.* Rings of anionic amino acids as structural determinants of ion selectivity in the acetylcholine receptor channel. *Proc R. Soc. Lond. B* **244,** 69–79 (1991).

24. Cohen, B. N., Labarca, C., Davidson, N. & Lester, H. A. Mutations in M2 alter the selectivity of the mouse nicotinic acetylcholine receptor for organic and alkali metal cations. *J. Gen. Physiol.* **100,** 373–400 (1992).
25. Corringer, P. J. *et al.* Mutational analysis of the charge selectivity filter of the alpha7 nicotinic acetylcholine receptor. *Neuron* **22,** 831–843 (1999).
26. Gunthorpe, M. J. & Lummis, S. C. Conversion of the ion selectivity of the 5-HT(3a) receptor from cationic to anionic reveals a conserved feature of the ligand-gated ion channel superfamily. *J. Biol. Chem.* **276,** 10977–10983 (2001).
27. Imoto, K. *et al.* Rings of negatively charged amino acids determine the acetylcholine receptor channel conductance. *Nature* **335,** 645–648 (1988).
28. Revah, F. *et al.* Mutations in the channel domain alter desensitization of a neuronal nicotinic receptor. *Nature* **353,** 846–849 (1991).
29. Beckstein, O. & Sansom, M. S. A hydrophobic gate in an ion channel: the closed state of the nicotinic acetylcholine receptor. *Phys. Biol.* **3,** 147–159 (2006).
30. Cymes, G. D., Ni, Y. & Grosman, C. Probing ion-channel pores one proton at a time. *Nature* **438,** 975–980 (2005).

Supplementary Information is linked to the online version of the paper at www.nature.com/nature.

Acknowledgements We thank I. Toth from the Scottish Crop Research Institute for providing g-DNA of *E. chrysanthemi*, B. Blattmann and A. Haisch for assistance with crystal screening, D. Sargent for help with Xe derivatization, C. Schulze-Briese and the staff of the X06SA beamline for support during data collection, the Protein Analysis Group at the Functional Genomics Center of the University of Zürich for help with mass spectrometry, R. MacKinnon for comments on the manuscript and members of the Dutzler laboratory for help in all stages of the project. Data collection was performed at the Swiss Light Source of the Paul Scherrer Institute. This work was supported by a grant from the National Center for Competence in Research in Structural Biology and the EMBO Young Investigator Program to R.D. R.J.C.H. is affiliated with the Molecular Life Sciences Ph.D. Program of the University/ETH Zürich.

Author Contributions R.D. and R.J.C.H. designed the project. R.J.C.H. performed all experiments. R.D. assisted in data collection, structure determination and electrostatic calculations. R.D. and R.J.C.H. jointly wrote the manuscript.

Author Information Coordinates have been deposited in the Protein Data Bank under code 2vl0. Reprints and permissions information is available at www.nature.com/reprints. Correspondence and requests for materials should be addressed to R.D. (dutzler@bioc.uzh.ch).

METHODS

Expression and purification. The gene encoding ELIC was cloned into a modified pET26b vector (Novagen) where it was fused to the C terminus of MBP, generating a construct with the pelB signal sequence followed by a $(His)_{10}$-Tag, MBP, a *Herpes simplex* (HRV) 3C protease site (GE Healthcare) and the ELIC sequence. BL21(DE3) cells transformed with this construct were grown at 37 °C in TB medium containing 50 mg l^{-1} kanamycin to an optical density $(OD)_{600}$ of about 1.6–1.8. Expression was induced by addition of 0.2 mM IPTG overnight at 20 °C. All following steps were performed at 4 °C. Cells were harvested and lysed with an Emulsiflex high-pressure homogenizer (Avestin) in 50 mM Na-Phosphate (pH 8.0), 150 mM NaCl (buffer A), with the addition of 1 mM phenylmethyl sulfonyl fluoride (PMSF), 20 μg ml^{-1} DNase I, 1 mg ml^{-1} lysozyme, 1 μg ml^{-1} pepstatin and 1 μg ml^{-1} leupeptin. The lysate was cleared by low-spin centrifugation. Membranes were isolated by ultracentrifugation and the proteins were extracted in buffer A containing 2% n-undecyl-β-d-maltoside (UDM, Anatrace, Inc.). After centrifugation, the protein was purified by affinity-chromatography on a Ni-NTA column (Qiagen). The purified MBP-ELIC-fusion protein was digested with HRV 3C protease to cleave the His_{10}-MBP protein and dialysed against 10 mM phosphate (pH 8.0), 150 mM NaCl and 3 mM UDM (buffer B). His_{10}-MBP was subsequently removed from solution by binding to Ni-NTA resin. ELIC was concentrated and subjected to gel filtration on a Superdex 200 column (GE Healthcare) in buffer B. The protein peak corresponding to the ELIC pentamer was pooled and concentrated to 10 mg ml^{-1} and used for crystallization. For reconstitution into liposomes, an additional anion exchange purification step (POROS HQ, Applied Biosystems) was introduced before gel filtration. For preparation of selenomethionine-labelled protein, cells were grown in minimal medium containing 50 mg l^{-1} selenomethionine, and SeMet-ELIC was purified as described.

Crystallization. ELIC was crystallized in sitting drops at 4 °C. Crystals were obtained by mixing protein containing additional 0.5 mg ml^{-1} *E. coli* polar lipids (Avanti Polar Lipids, Inc.) in a 1:1 ratio with reservoir solution containing 200 mM $(NH_4)_2SO_4$, 50 mM ADA (pH 6.5) and 10–15% PEG 4000. For cryo-protection, the crystals were transferred into mother liquor containing 30% glycerol or ethyleneglycol and flash-frozen in liquid propane. For Xe derivatization, crystals were exposed to a Xe atmosphere at 20 bar for 10 min and frozen as described above. For soaking with Cs^+, Tl^+ and Rb^+ ions, crystals were incubated in mother liquor where $(NH_4)_2SO_4$ and NaCl was replaced by the respective sulphate salt for 1 h and flash frozen by addition of 30% ethylene glycol.

Structure determination. All data sets were collected on frozen crystals on the X06SA beamline at the Swiss Light Source of the Paul Scherrer Institut on a PILATUS detector (Dectris). The data were indexed, integrated and scaled with XDS[31] and further processed with CCP4 programs[32]. The structure was determined by the SIRAS method using the anomalous and isomorphous contributions of a Se-Met derivative that also served as native data set and a Xe derivative. The Se sites were identified with SHELX C and D[33,34] and were used to calculate initial phases for the identification of the Xe sites by difference Fourier techniques. Se and Xe sites were refined in SHARP[35], and phases were improved by solvent flattening and extended to 3.3 Å by tenfold NCS symmetry averaging in DM[36]. The model was built in O[37] and initially refined by maintaining strict tenfold NCS constraints in CNS[38]. In later stages, the strict constraints were loosened and restraint individual B-factors were refined. R and R_{free} were monitored throughout. R_{free} was calculated by selecting 5% of the reflection data in thin slices that were omitted in refinement. The final model has R/R_{free} values of 26.3% and 27.4%, good geometry and no outliers in the Ramachandran plot. The pore radii of ELIC and nAChR were calculated with the program HOLE[39]. The molecular surface was calculated with MSMS[40].

Reconstitution, electrophysiological recordings and data analysis. ELIC was reconstituted into *E. coli* polar lipids that were previously solubilized in reconstitution buffer (450 mM KCl, 25 mM citric acid, 25 mM phosphoric acid, pH 7.0) containing 35 mM CHAPS in a protein-to-lipid ratio of 5 μg mg^{-1} lipids with a final lipid concentration of 15 mg ml^{-1}. The detergent was removed by dialysis, and liposomes were frozen in liquid nitrogen and stored at −80 °C. Liposomes containing ELIC were fused to bilayers formed from POPE/POPG lipids (Avanti) and recorded in a horizontal planar lipid bilayer system as previously described[41]. Electrodes were connected to the respective bath solutions through salt bridges. Solutions containing Na^+ ions were prepared with 10 mM Na_2HPO_4 as buffer. NaCl was added to reach the desired Na^+ concentration. Solutions containing K^+ ions were prepared in a similar way but with K_2HPO_4 and KCl instead. Cs^+ solutions were prepared by mixing 10 mM Na_2HPO_4 and 400 mM CsCl. For all solutions, pH was adjusted to 7.0 with HCl. Macroscopic currents were recorded with an Axopatch amplifier 200B (Axon Instruments, Inc.). Data were sampled at 50 μs, filtered at 200 Hz and analysed with Clampfit (Axon Instruments, Inc.).

Poisson–Boltzmann calculations. Electrostatic potential was calculated by solving the linearized Poisson–Boltzmann equation in CHARMM[42,43] on a 110 Å × 110 Å × 150 Å grid (1 Å grid spacing) followed by focusing on a 90 Å × 90 Å × 140 Å grid (0.5 Å grid spacing). Partial protein charges were derived from the Param19 extended hydrogen atom forcefield. Polar hydrogen positions were generated in CHARMM. ELIC was assigned a dielectric constant of 2. Its transmembrane region was embedded in a slab of 30 Å thickness ($\varepsilon = 2$), representing the membrane that contained a cylindrical hole ($r = 8$ Å, $\varepsilon = 80$) around the water-filled pore region and was surrounded by an aqueous environment ($\varepsilon = 80$). The concentration of mobile ions was set to zero.

31. Kabsch, W. Automatic processing of rotation diffraction data from crystals of initially unknown symmetry and cell constants. *J. Appl. Cryst.* **26,** 795–800 (1993).
32. Collaborative Computational Project, Number 4. The *CCP*4 suite: programs for X-ray crystallography. *Acta Crystallogr. D* **50,** 760–763 (1994).
33. Pape, T. & Schneider, T. R. HKL2MAP: a graphical user interface for phasing with SHELX programs. *J. Appl. Cryst.* **37,** 843–844 (2004).
34. Schneider, T. R. & Sheldrick, G. M. Substructure solution with SHELXD. *Acta Crystallogr. D* **58,** 1772–1779 (2002).
35. de La Fortelle, E. & Bricogne, G. in *Methods in Enzymology* (eds Carter, C. W. & Sweet, R. M.) 492–494 (Academic, New York, 1997).
36. Cowtan, K. An automated procedure for phase improvement by density modification. *Joint CCP4 ESF-EACBM Newslett. Protein Crystallogr.* **31,** 34–38 (1994).
37. Jones, T. A., Zou, J. Y., Cowan, S. W. & Kjeldgaard, M. Improved methods for building protein models in electron density maps and the location of errors in these models. *Acta Crystallogr. A* **47,** 110–119 (1991).
38. Brunger, A. T. *et al.* Crystallography & NMR system: a new software suite for macromolecular structure determination. *Acta Crystallogr. D* **54,** 905–921 (1998).
39. Smart, O. S., Neduvelil, J. G., Wang, X., Wallace, B. A. & Sansom, M. S. HOLE: a program for the analysis of the pore dimensions of ion channel structural models. 14, 354–360 *J. Mol. Graph.* **14,** 354–360, 376 (1996).
40. Sanner, M. F., Olson, A. J. & Spehner, J. C. Reduced surface: an efficient way to compute molecular surfaces. *Biopolymers* **38,** 305–320 (1996).
41. Nimigean, C. M. & Miller, C. Na^+ block and permeation in a K^+ channel of known structure. *J. Gen. Physiol.* **120,** 323–335 (2002).
42. Brooks, B. R. *et al.* CHARMM: a program for macromolecular energy, minimization, and dynamics calculations. *J. Comput. Chem.* **4,** 187–217 (1983).
43. Im, W., Beglov, D. & Roux, B. Continuum salvation model: electrostatic forces from numerical solutions to the Poisson–Bolztmann equation. *Comput. Phys. Commun.* **111,** 59–75 (1998).